AIAA JOURNAL
Vol. 31, No. 11, November 1994

Laplace Interaction Law for the Computation of Viscous Airfoil Flow in Low- and High-Speed Aerodynamics

F. Arnold*
Deutsche Aerospace Airbus GmbH, Bremen 28183, Germany
and
F. Thiele†
Technical University Berlin, 10623 Berlin, Germany

A new interaction law that accelerates convergence of interactive boundary-layer methods is presented. The law is derived from the Laplace equation and allows the automatic implementation of the Kutta condition for lifting airfoil flows. The accurate influence coefficients of the Laplace interaction law (LIL) facilitate efficient prediction of high-lift flows about multi-element airfoils by direct numerical simulation. Taking into account suitable turbulent closure relations for boundary-layer equations, a fast and reliable computer code has been developed for industrial applications at Deutsche Aerospace Airbus. Very fast convergence and good agreement of calculated results with experiments are observed over a reasonable range of multi-element airfoil flows up to maximum lift. The LIL coupling technique can also be extended to transonic flows. A quasisimultaneous iteration procedure, similar to well-known thin-airfoil coupling techniques follows, and accelerated convergence is obtained using the more appropriate influence coefficients of LIL.

Introduction

THE aerodynamic design of modern transport aircraft wings is essentially based on numerical methods, and the demand for more efficient flow simulation codes is rapidly increasing.[1] Currently, a complete and accurate simulation of the flow behavior over complex wing configurations (fuselage-wing-pylon-engine configuration at high lift) is not possible using available computer codes. After previous experience in calculating three-dimensional wing flows by interactive boundary-layer (IBL) methods, more and, one hopes, better results are expected in the future from new three-dimensional Navier-Stokes codes.[2] Here, the main problems are the generation of suitable grids and the modeling of turbulence, especially in the wake flow.

Many computer codes already exist for the two-dimensional case, however.[2-4] These include the more recent two-dimensional Navier-Stokes methods[2] and IBL methods[3] mainly developed in the early 1980s. The Navier-Stokes methods are generally not used in industrial aerodynamic design for two reasons. First, they suffer from poor turbulence modeling and thus do not produce better results than IBL methods. Second, they have much higher application costs. IBL methods are better for aerodynamic design tools. Using a suitable boundary-layer closure and a strong coupling technique, one can also predict airfoil flows with massive separation.[5]

The first step in the strong matching of inviscid and boundary-layer solutions was the semi-inverse coupling technique. Carter[6] and Le Balleur[7] pointed the way to predicting separated flows by coupling a direct inviscid solution with an inverse boundary-layer solution. Computer codes based on these techniques show good convergence behavior for weak interactions, but they need considerable underrelaxation for strong interacting flows to avoid divergence. Semi-inverse methods become slow and difficult to handle for flows with large separation. Quasisimultaneous coupling techniques, developed by Veldman[8] and Davis and Werle,[9] for example, accelerate convergence. In these techniques the viscous approximation becomes more appropriate by the simultaneous solution of the boundary-layer equations together with a simplified interaction law for the inviscid flow based on the thin-airfoil theory. The convergence of the coupling of the improved boundary-layer solution with the complete inviscid solution depends on the accuracy of the interaction law. Several investigations have been done to modify interaction law influence coefficients to accelerate IBL convergence. Veldman et al.[10] developed influence coefficients for antisymmetric flows; Davis and Werle[9] investigated integration by parts of the thin-airfoil equation; Edwards and Carter[11] and Sorensen[12] considered the displacement effect of the airfoil contour within the interaction law, and Rothmayer[13] demonstrated faster convergence by using the inversion formula of thin-airfoil theory that automatically implements the Kutta condition.

In this paper, the idea of improving interaction law influence coefficients is extended to a direct numerical solution for low-subsonic airfoil flows. To obtain accurate influence coefficients, we replace the thin-airfoil equation by the Laplace equation. A multi-element airfoil panel method[14] is used to express the Laplace equation in terms of two-dimensional velocity components. The resulting Laplace interaction law (LIL) due to Arnold[15] comprises an appropriate inviscid solution for lifting airfoil flows. Based on the fact that only the influence coefficient matrix differs from the thin-airfoil approach, the coupling of LIL and boundary-layer equations is as simple as that for the thin-airfoil interaction law.

The new coupling technique is termed "local-simultaneous" because the boundary-layer equations are linearized locally. The influences from the whole flow domain on the local viscous solution are iteratively determined. It has been shown before, from the triple deck theory,[16] that this elliptical interaction phenomenon is of less importance than the local viscous-inviscid interaction.

In the current work, the derivation of LIL and the local-simultaneous coupling technique using an integral boundary-layer method[17] are shown for low-subsonic multi-element airfoil flows. For the resulting computer code, viscous-inviscid low-speed method for multi-element airfoils (VILMA),[18] convergence behavior is presented and computational results are discussed by comparison with wind-tunnel experiments. In addition, an example of extending LIL application to transonic airfoil flows within a quasisimultaneous coupling technique is given. A method[19] for transonic flows over single-element airfoils, developed at Deutsche Aerospace Airbus, has been taken for the LIL coupling of a finite difference boundary-layer method[20] with a full potential method.[21] In the transonic flow solver, the implemented Veldman thin-airfoil interaction law was easily substituted by LIL to demonstrate principle convergence behavior.

Received July 10, 1993; presented as Paper 93-3462 at the AIAA 11th Applied Aerodynamics, Monterey, CA, Aug. 9–13, 1993; revision received May 9, 1994; accepted for publication May 11, 1994.

*Research Scientist, Theoretical Aerodynamics Branch. Member AIAA.
†Professor, Hermann-Föttinger-Institut für Thermo- und Fluiddynamik.

Laplace Interaction Law

In linear potential theory the Laplace equation is satisfied by the singularity distribution of constant source strength σ and linear vorticity strength γ over each panel i along the surface of each airfoil element. A system of $2n$ linear equations for n tangential inviscid velocities u_{IW_i} and for the streamline condition of n normal velocities $v_{IW_i} = 0$ at the n panel centers follows:

Inviscid:

$$v_{IW_i} = 0 = v_{\infty_i} - v_{\mathrm{MOD}_i} + \sum_{j=1}^{n} \Sigma_{ij}^{N} \sigma_{I_j} + \sum_{j=1}^{n+1} \Gamma_{ij}^{N} \gamma_j$$

$$\text{for} \quad i = 1, \ldots, n \tag{1}$$

$$u_{IW_i} = u_{\infty_i} + \sum_{j=1}^{n} \Sigma_{ij}^{T} \sigma_{I_j} + \sum_{j=1}^{n+1} \Gamma_{ij}^{T} \gamma_j$$

$$\text{for} \quad i = 1, \ldots, n \tag{2}$$

The source term σ_I compensates v_∞ and induces v_{MOD} to simulate blunt trailing edges. It is substituted by $\sigma = v/2\pi$. An additional equation is obtained from the Kutta condition of equal tangential velocities at the trailing edge:

Kutta condition (inviscid):

$$0 = u_{IW_{i=LHU}} - u_{IW_{i=LHO}} \tag{3}$$

where LHU denotes the lower side and LHO the upper side trailing-edge index. For $n + 1$ unknown vorticities γ at the panel boundaries, n equations for v_{IW} and the Kutta equation need to be solved. Then the velocities u_{IW} on n panel centers are obtained.

In viscous flow, however, the normal velocities describe the boundary-layer and wake displacement effect by the virtual outblow concept[22,23]:

$$v_{IW} = \frac{1}{\rho_e} \frac{\mathrm{d}(\rho_e u_e \delta_1)}{\mathrm{d}x} \tag{4}$$

The consideration of outblow velocities on the surface and on the wake-dividing streamline leads to a change in u_{IW} of Δu_{IW}, and the inviscid equation system (1) and (2) and the Kutta condition (3) are extended by viscous boundary conditions:

Viscous:

$$v_{IW_i} = v_{\infty_i} - v_{\mathrm{MOD}_i} + \sum_{j=1}^{n} \Sigma_{ij}^{N} \sigma_{I_j} + \sum_{j=1}^{n+n_w} \Sigma_{ij}^{N} \sigma_{V_j} t + \sum_{j=1}^{n+1} \Gamma_{ij}^{N} \gamma_j$$

$$\text{for} \quad i = 1, \ldots, n \tag{5}$$

$$(u_{IW} + \Delta u_{IW})_i = u_{\infty_i} + \sum_{j=1}^{n} \Sigma_{ij}^{T} \sigma_{I_j} + \sum_{j=1}^{n+n_w} \Sigma_{ij}^{T} \sigma_{V_j} + \sum_{j=1}^{n+1} \Gamma_{ij}^{T} \gamma_j, \qquad \text{for} \quad i = 1, \ldots, n + 2n_w \tag{6}$$

Kutta condition (viscous):

$$0 = (u_{IW} + \Delta u_{IW})_{i=LHU} - (u_{IW} + \Delta u_{IW})_{i=LHO} \tag{7}$$

For this purpose the wake-dividing streamline is covered with $2n_w$ panels. These are equal for the lower and upper half-wake and carry only one distribution σ_V of constant source strengths for both. Thus, from n_w source strengths in the wake-panel centers, $2n_w$ tangential and normal velocities are obtained for the lower and upper half-wake.

The velocity $(u_{IW} + \Delta u_{IW})$ is termed the "equivalent potential velocity" and is calculated on the airfoil surface and on the wake-dividing streamline, too. Assuming that the equivalent potential velocity is constant in the boundary-layer cross section, the velocity u_e at the boundary-layer edge is given by

$$u_e = u_{IW} + \Delta u_{IW} \tag{8}$$

In Eqs. (5–7) the elimination of vorticities γ by the inversion of the matrix $|\Gamma^N|$ and the substitution of sources σ by $\sigma = v/2\pi$ on the surface and by $\sigma = \Delta v/2\pi$ in the wake [$\Delta v_{IW} = v_{IW}$(upper half-wake) $- v_{IW}$(lower half-wake)] leads to a system of $n + 2n_w$ linear equations for u_e and v_{IW}:

Laplace interaction law (LIL):

$$u_{e_i} = u_{IW_i} + \sum_{j=1, j\neq i}^{n+2n_w} E_{ij} v_{IW_j} + E_{ii} v_{IW_i}$$

$$\text{for} \quad i = 1, \ldots, n + 2n_w \tag{9}$$

with the LIL influence coefficient matrix $|E|$ of magnitude $(n + 2n_w)^2$ for $n + 2n_w$ panels:

$$|E| = |\Gamma^T||\Gamma_{\mathrm{INV}}^N| + \frac{1}{2\pi}(|\Sigma^T| - |\Gamma^T||\Gamma_{\mathrm{INV}}^N||\Sigma^N|) \tag{10}$$

The subscript INV denotes the inverse matrix, and u_{IW} is identically the inviscid solution of Eqs. (1–3) with extension of Eq. (2) into the wake. In the LIL, u_{e_i} accurately takes into account influences from the local inviscid solution u_{IW_i}, from the local outblow velocity v_{IW_i}, and from all other outblow velocities

$$\sum_{j=1, j\neq i}^{n+2n_w} E_{ij} v_{IW_j}$$

on the remaining panels j. The LIL satisfies the Laplace equation incorporating equal boundary-layer edge velocities at the trailing edge and equal wake-edge velocities downstream. It could be extended for simulating wake curvature effects by covering the wake-dividing streamline with vorticity strengths and by modifying the Kutta condition. But the computational effort would be increased due to the inversion of the matrix $|\Gamma^N|$ of magnitude $(n + 2n_w)^2$ instead of n^2.

For multi-element airfoil problems consisting of k elements and described by $m = n_1 + 2n_{w_1} + \cdots + n_k + 2n_{w_k}$ panels, we obtain m LIL equations, Eqs. (9) from Eqs. (5) and (6) and from k Kutta conditions (7). The magnitude of the matrix $|E|$ is now m^2.

The implementation of LIL depends on the solution method applied for the boundary-layer simulation. In the following section an example of the implementation of an integral boundary-layer method is given for low-speed flows, and in a later section the implementation of a finite difference boundary-layer method is shown.

Low-Speed Flows

Local-Simultaneous Coupling of LIL with Integral Boundary-Layer Method

In the following equations the subscript i runs from 1 to $m = n + 2n_w$. For the coupling of LIL with the integral boundary-layer method the derivative of the LIL equation, Eq. (9), with respect to x yields

$$\frac{\mathrm{d}u_{e_i}}{\mathrm{d}x} = \frac{\mathrm{d}u_{IW_i}}{\mathrm{d}x} + \frac{\mathrm{d}}{\mathrm{d}x}\left(\sum_{j=1}^{m} E_{ij} v_{IW_j}\right) \tag{11}$$

Using central difference formulas for nonequidistant steps gives the discretized formulation of LIL:

$$\frac{\mathrm{d}u_{e_i}}{\mathrm{d}x} = c_{1_i} + c_{2_i} v_{IW_i} \tag{12}$$

with

$$c_{1_i} = \lambda_{I_i} \frac{\mathrm{d}u_{IW_i}}{\mathrm{d}x} + \lambda_{V_i} \sum_{j=1, j\neq i}^{m} D_{ij} v_{IW_j}$$

$$c_{2_i} = D_{ii} \tag{13}$$

$$D_{ij} = a_i E_{i-1,j} + b_i E_{ij} + c_i E_{i+1,j}$$

$$a_i = \frac{\Delta x_i}{(\Delta x_{i-1} - \Delta x_i)\Delta x_{i-1}}$$
$$b_i = \frac{(\Delta x_{i-1})^2 - (\Delta x_i)^2}{(\Delta x_{i-1} - \Delta x_i)\Delta x_{i-1}\Delta x_i} \quad (14)$$
$$c_i = \frac{-\Delta x_{i-1}}{(\Delta x_{i-1} - \Delta x_i)\Delta x_i}$$

$$\Delta x_i = x_i - x_{i+1} < 0, \qquad \Delta x_{i-1} = x_i - x_{i-1} > 0 \quad (15)$$

$$\lambda_I, \lambda_V = \begin{cases} +1: i > LST & \text{(upper surface/half-wake)} \\ 0: i = LST & \text{(stagnation point)} \\ -1: i < LST & \text{(lower surface/half-wake)} \end{cases} \quad (16)$$

where LST refers to the stagnation point index. For the calculation of the LIL influence coefficient matrix $|E|$ the panel method from Jakob[14] was adapted. Figure 1 shows that for one airfoil element the discretized LIL influence coefficient matrix $|D|$ is diagonally dominant with small disturbances at the stagnation point and in the trailing-edge region. Diagonal dominance is one requirement for fast convergence.[8]

For calculating the boundary-layer flow over multi-element airfoils, an integral method[17] is used that is based on the integral equations of Whitfield et al.[24]:

$$\frac{1}{H_{12}}\frac{\partial H_{12}}{\partial \bar{H}_{12}}\frac{\partial \bar{H}_{12}}{\partial x} - \left(1 + H_{12} - \frac{\partial H_{12}}{\partial M_e}\frac{M_e F_c^2}{H_{12}}\right) \times \frac{1}{u_e}\frac{\partial u_e}{\partial x} - \frac{1}{A}\frac{\mathrm{d}A}{\mathrm{d}x} = \frac{c_f}{2\delta_2} \quad (17)$$

$$\frac{\partial H_{32}}{\partial \bar{H}_{12}}\frac{1}{H_{32}}\frac{\partial \bar{H}_{12}}{\partial x} + \left(1 + 2\frac{H_{42}}{H_{32}} - H_{12} + \frac{\partial H_{32}}{\partial M_e}\frac{M_e F_c^2}{H_{32}}\right) \times \frac{1}{u_e}\frac{\partial u_e}{\partial x} = \frac{c_d}{\delta_2 H_{32}} - \frac{c_f}{2\delta_2} \quad (18)$$

with

$$A = \rho_e u_e \delta_1, \qquad F_c^2 = 1 + \frac{\kappa - 1}{2} M_e^2 \quad (19)$$

and the closure relations of Drela.[25]

The elimination of $\partial \bar{H}_{12}/\partial x$ and substitution of $(1/\rho_e)(\mathrm{d}A/\mathrm{d}x)$ by v_{IW} from Eq. (4) gives

$$\frac{\mathrm{d}u_e}{\mathrm{d}x} = c_3 - c_4 v_{IW} \quad (20)$$

with

$$c_3 = \frac{[(E + C)(c_f/2)] - (C c_d/H_{32})}{(\delta_2 \cdot FN)}, \qquad c_4 = (\rho_e E)/(A \cdot FN) \quad (21)$$

$$FN = B \cdot E - C \cdot D \quad (22)$$

$$B = \left(1 + H_{12} - \frac{M_e F_c^2}{H_{12}}\frac{\partial H_{12}}{\partial M_e}\right)\frac{1}{u_e}, \qquad C = -\frac{1}{H_{12}}\frac{\partial H_{12}}{\partial \bar{H}_{12}} \quad (23)$$

$$D = \left(1 + 2\frac{H_{42}}{H_{32}} - H_{12} + \frac{M_e F_c^2}{H_{32}}\frac{\partial H_{32}}{\partial M_e}\right)\frac{1}{u_e}, \qquad E = \frac{1}{H_{32}}\frac{\partial H_{32}}{\partial \bar{H}_{12}} \quad (24)$$

If the panel centers i are not identical with the boundary-layer mesh, the LIL coefficients c_1 and c_2 must be interpolated. The local-simultaneous solution for the two unknowns $\mathrm{d}u_e/\mathrm{d}x$ and v_{IW} is obtained from the system of two linear equations, Eqs. (12) and (20), which may be solved by direct elimination. Afterwards, the velocity

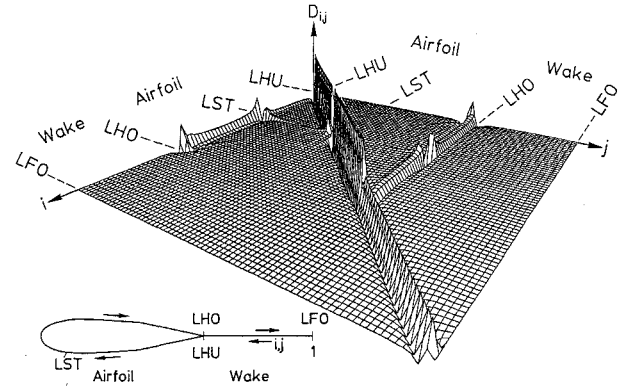

Fig. 1 Structure of influence coefficient matrix of the Laplace interaction law.

at the boundary-layer edge u_e and the boundary-layer displacement thickness δ_1 are determined from integration by the trapezoidal rule. The coefficients c_3 and c_4, however, depend on the local boundary-layer solution. The nonlinearity of the boundary-layer equations is dealt with by iterative calculation of the local-simultaneous solution.

The computer code VILMA[18] was developed from the previous theory. This method consists of a panel method for two-dimensional inviscid flows over multi-element airfoils and allows consideration of the infinite conical swept wing and freestream curvature conditions. The implemented boundary-layer method consists of Drela's[25] closure relations for nonequilibrium boundary layers and has been extended for leading-edge stall analysis by the van Ingen[26] transition-bubble model and the Goradia-Lyman[27] criterion for bubble bursting. Transition for attached flows is predicted by the Granville[28] criterion or is fixed a priori. In the latter case the transition strip influence is considered by increasing the momentum thickness. Confluences of boundary layers and wakes are not considered.

Iteration Process

The calculation starts from the potential solution using a panel method for the LIL coefficients c_1 and c_2, with $v_{IW} = 0$. Then the boundary-layer calculation begins at the stagnation point of the first element using a Falkner-Skan solution and continues in the laminar flow region for given pressures obtained from the inviscid solution. At laminar separation, or transition, the local-simultaneous solutions follow for the turbulent flow. For given coefficients c_1 and c_2 from LIL and c_3 and c_4 from the upstream position, the local values of u_e and δ_1 are calculated. Then the boundary-layer coefficients c_3 and c_4 are updated from the new u_e and δ_1 values, and the local-simultaneous solution is repeated. During the validation of the VILMA code it was observed that only two of these local updates are required to provide sufficiently accurate results. Once the solutions $\mathrm{d}u_e/\mathrm{d}x$ and v_{IW} are calculated for all airfoil elements and its wakes, the boundary-layer sweep is finished.

The elliptical effect of LIL is considered in a global iteration process. New LIL coefficients c_1 and c_2 are calculated from the solution of the previous boundary-layer sweep. For adjusting wake-dividing streamline positions during the iteration, the local inviscid velocities u_{IW} and the components of the coefficient matrix $|E|$ relating to the wake region must be corrected. On the surfaces the inviscid solution and the matrix remain unchanged, and only the new outblow velocities must be considered. For the new LIL coefficients c_1 and c_2, the next boundary-layer sweep follows. The converged solution is obtained when the required accuracies for the lift coefficient and the local displacement thicknesses are achieved.

The behavior of the iteration procedure is studied for some typical test cases of incompressible high-lift flows about single- and multi-element airfoils with Reynolds numbers ranging from 1.6×10^6 to 6×10^6. The local-simultaneous technique implemented in VILMA is compared with the semi-inverse technique of Carter.[6] Figure 2 shows the required number of global iterations and the CPU times using an IBM 3090 computer for single-, two-, three, and four-element airfoils for the whole lift polar. For all of these test cases, VILMA clearly shows a smaller number of iterations and faster CPU

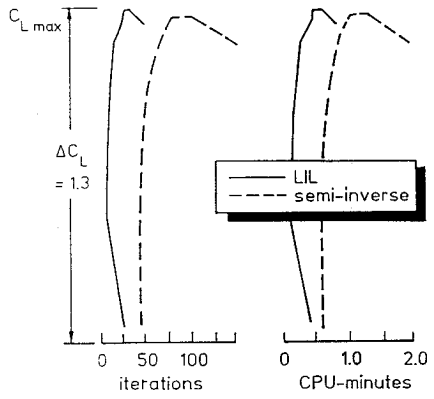

a)

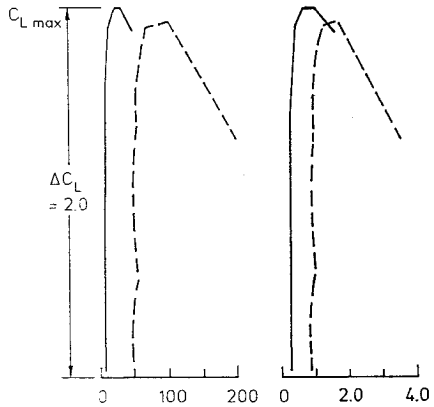

b)

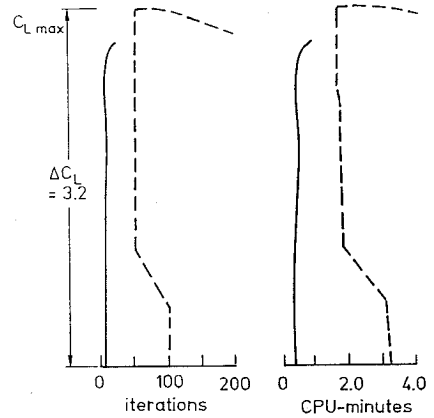

c)

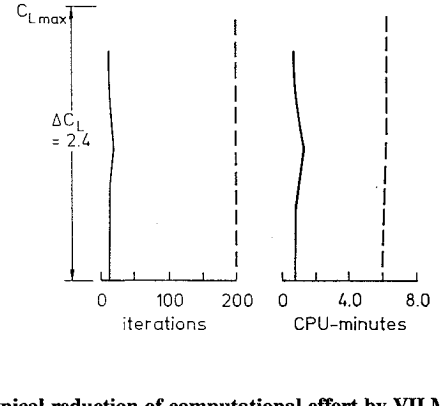

d)

Fig. 2 Typical reduction of computational effort by VILMA calculations, $M_\infty < 0.2$, $10^6 < Re_\infty < 6 \times 10^6$, for a) single-element airfoils, b) two-element airfoils, c) three-element airfoils, and d) four-element airfoils.

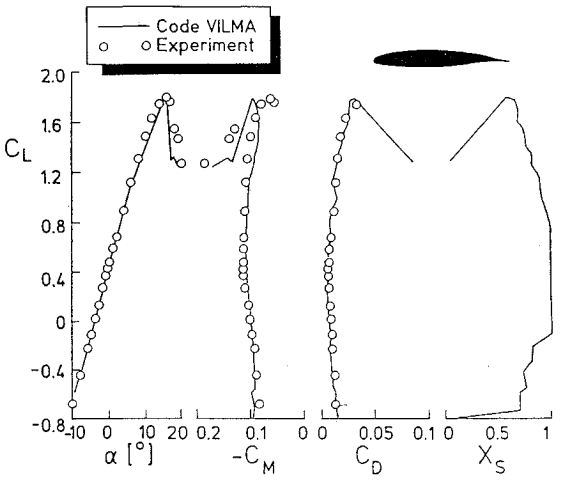

Fig. 3 Aerodynamic polars and separation behavior for GA(W)-2 single-element airfoil at $M_\infty = 0.15$ and $Re_\infty = 3 \times 10^6$, ($x_S = x/c$ at beginning of turbulent separation).

times. The higher effort in building the LIL influence coefficient matrix at the beginning of calculation is completely compensated by the very fast convergence of the numerical solution technique. Below maximum lift, the computational effort is nearly constant. At maximum lift, the increase in computational effort is clearly less than for the semi-inverse technique. All of the results of VILMA are performed without relaxation, whereas the semi-inverse technique requires relaxation of about 25% for single-element airfoils and up to 95% (i.e., 95% old solution and 5% new solution) for four-element airfoils to avoid divergence.

These investigations are performed for flows with moderate boundary-layer separation. Flows with massive separation on the flaps, which are characteristic of landing configurations with very high flap deflection angles, can also be calculated with VILMA. But investigations for multiple-slotted flaps up to five-element airfoils in landing configuration with total flap deflection angles of about 60 deg sometimes show poor convergence due to numerical oscillations in the massive separated flow domain.

Aspects of Application

To obtain information about the quality of the predicted results, we compared them with experimental wind-tunnel data over a reasonable range of high-lift flows. Aerodynamic polars are shown for the single-element airfoil GA(W)-2, for the two-element airfoil NLR7301 (wing + flap) either with a large gap or with a small gap, and for the takeoff and landing configurations of both the GARTEUR three-element airfoil (slat + wing + flap) and the Deutsche Aerospace Airbus four-element airfoil DA4E (slat-wing-flap + tab). For the latter case, which is the most ambitious one, typical pressure distributions are shown as well.

Single-Element Airfoil

In Fig. 3 the aerodynamic polars and the separation behavior are presented for the test case GA(W)-2. Greater discrepancies of the computational results from the experimental data[29] only occur for the maximum lift region of the curves, which can also be confirmed by other single-element flow calculations. The pressure distributions are not shown in this paper, but they are in good agreement below maximum lift. For low-lift, turbulent separation begins at the upper surface trailing edge and moves upstream with increasing lift. At maximum lift it is located at about 50% chord and moves straight upstream to the leading edge at the beginning of stall.

Two-Element Airfoil

For the two-element airfoil NLR7301 wing plus flap shown in Fig. 4, the calculated polars agree reasonably well with the experimental data[30] below maximum lift. The maximum lift region is overestimated by the calculations for the larger gap, as well as for the smaller gap. The experiments show a reduction of maximum lift of about $\Delta c_L = 0.16$ when the gap size is reduced from the

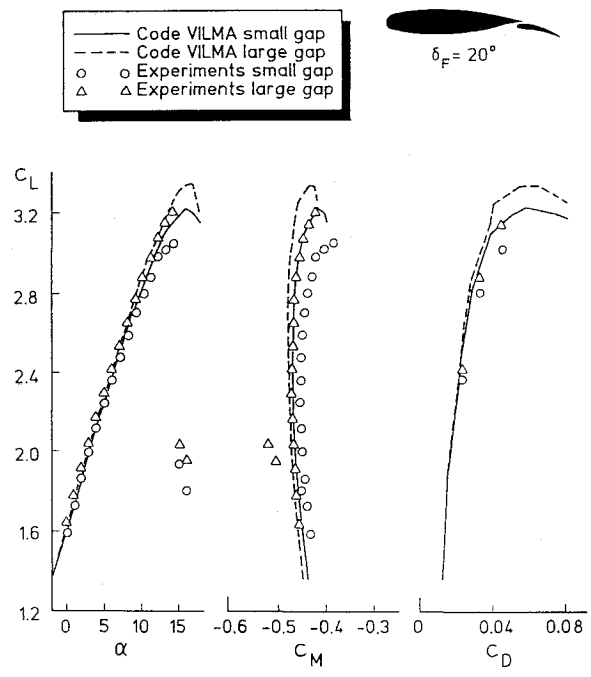

Fig. 4 Aerodynamic polars for NLR7301 two-element airfoil at M_∞ = 0.2 and $Re_\infty = 2.5 \times 10^6$.

larger to the smaller one. VILMA calculates a reduction of about $\Delta c_L = 0.12$ as well. Already for 13-deg angle of attack, the calculated displacement thicknesses of the wing wake over the flap are underestimated, whereas the wing and flap boundary-layer data agree well with experimental data. It follows that the pressure distributions on the wing are in general agreement for the small and the large gap. Discrepancies arise on the flaps due to the underestimation of the wing-wake displacement effect. Additionally, for the smaller gap the experiments show confluence on the flap upper surface, which is not a part of the calculations.

Three-Element Airfoil

The effects of wake displacement and confluence are of prime importance for airfoils with more elements. The pressure distribution on the element can be strongly influenced by the wakes of the upstream elements. As can be seen in Fig. 5 for the takeoff and landing configuration of the GARTEUR three-element airfoil (slat + wing + flap), the predicted results clearly show discrepancies from the measurements[31] for the maximum lift region. For smaller angles of attack, the shortcomings of not considering these effects in the computer code are less important, and the results show good agreement. It is remarkable that the changes of the flow parameters are described well by VILMA when the configuration is changing. From the takeoff to the landing configuration, the lift coefficient increases by about $\Delta c_L = 0.48$ in the experiments. VILMA calculates an increase of about $\Delta c_L = 0.42$. On the slat and wing, the predicted and measured pressure distributions generally agree below maximum lift. The results on the flaps in Fig. 6, however, show discrepancies again in spite of calculating a reasonable boundary-layer separation on the flap in the landing configuration. The total wake of the slat and the wing over the flap does not seem to be predicted adequately enough.

Four-Element Airfoil

The effects mentioned earlier are also valid for multi-element airfoils consisting of four or more elements. The four-element airfoil results shown in this section are representative for the multiple-slotted flaps applications of VILMA. For these test cases it is shown in Fig. 7 that the predicted results for the takeoff and landing configuration also agree well with experimental data[32] below maximum lift. Unfortunately, maximum lift is not measured but computational results show an increase in maximum lift for the landing configuration. For the takeoff configuration the code is stable and produces accurate results. For the landing configuration some oscillations in the polars

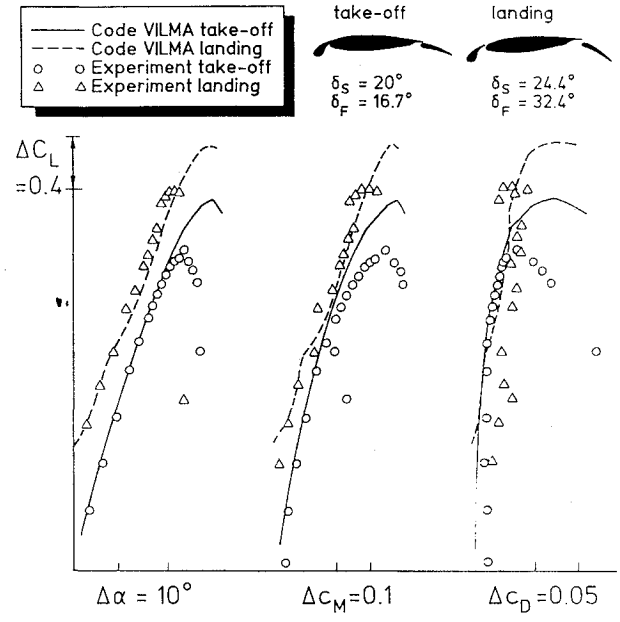

Fig. 5 Aerodynamic polars for GARTEUR three-element airfoil at M_∞ = 0.2 and $Re_\infty = 6 \times 10^6$.

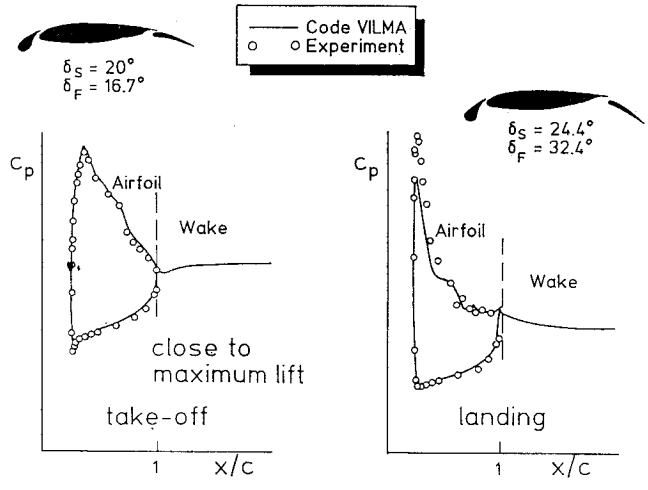

Fig. 6 Pressure coefficients on upper and lower surface of the flap of the GARTEUR three-element airfoil at M_∞ = 0.2 and $Re_\infty = 6 \times 10^6$.

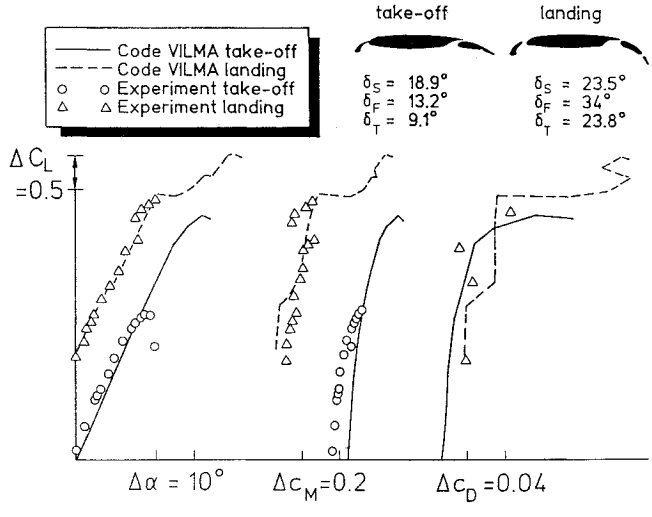

Fig. 7 Aerodynamic polars for DA4E four-element airfoil at M_∞ = 0.15 and $Re_\infty = 1.4 \times 10^6$.

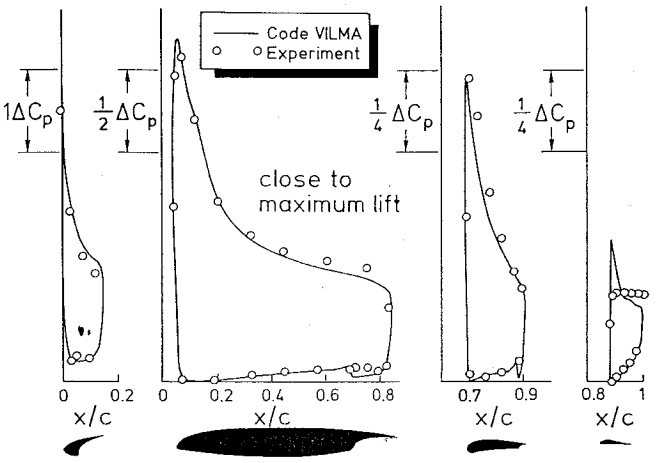

Fig. 8 Pressure coefficients on upper and lower surfaces of the DA4E four-element airfoil at $M_\infty = 0.15$ and $Re_\infty = 1.4 \times 10^6$, landing configuration.

occur, and the higher lift results are not reasonable. As can be seen from the pressure distributions in Fig. 8, massive separation begins near the leading edge of the tab upper surface and produces outblow velocities in the trailing-edge region of about $v_{IW} \approx 0.4u_\infty$. This makes the iteration of elliptical effects unstable as well. A relaxation for the global iteration may help and is currently under investigation.

High-Speed Flows

LIL Application for Quasisimultaneous Coupling Techniques

For the compressible case, the dependency of the inviscid flow quantities becomes nonlinear. Thus, the local-simultaneous coupling of LIL with the boundary-layer equations does not adequately describe the compressible flow. A major iteration process ν_I is additionally required that couples the LIL/boundary-layer solution with the complete inviscid solution.

Veldman et al.[10] proposed a difference formulation of the thin-airfoil interaction law for the quasisimultaneous coupling technique in high-speed applications. For the compressible flow the viscous solution at the boundary-layer edge u_{e_c} is obtained by the iteratively modified inviscid solution incorporating viscous effects u_{IVW_c} and an adjustable correction term Δu_{e_c}, which approaches $\Delta u_{e_c} = 0$ for the converged solution $u_{e_c} = u_{IVW_c}$:

$$u_{e_c}^{\nu_I} = u_{IVW_c}^{\nu_I} + \Delta u_{e_c}^{\nu_V} \tag{25}$$

The correction term Δu_{e_c} is described by the difference formulation of the interaction law. In the DA code[19] for transonic flows over single-element airfoils, the thin-airfoil interaction law was replaced by the more appropriate LIL to couple a finite difference boundary-layer method[20] with a full potential method[21] by a quasisimultaneous procedure.

The local difference of LIL between two successive boundary-layer sweeps ν_V is given from Eq. (9) for $m = n + 2n_w$ panels:

$$\Delta u_{e_{c_i}}^{\nu_V} = u_{e_i}^{\nu_V} - u_{e_i}^{\nu_V - 1} = K_i \sum_{j=1,\, j\neq i}^{m} E_{ij}\left(v_{IW_j}^{\nu_V} - v_{IW_j}^{\nu_V - 1}\right)$$

$$+ E_{ii}\left(v_{IW_i}^{\nu_V} - v_{IW_i}^{\nu_V - 1}\right) \tag{26}$$

where K is a Mach number correction (e.g., Prandtl-Glauert). Equation (26) requires that the potential solution u_{IW_i} and the LIL influence coefficient matrix $|E|$ remain unchanged during the boundary-layer iteration ν_V. For the consideration of wake-dividing streamline adjustments it is advisable to correct the LIL matrix $|E|$ for new wake positions in the next inviscid iteration step ν_I.

The implementation of Eq. (26) in Eq. (25) leads to the compressible formulation of LIL:

$$u_{e_{c_i}}^{\nu_I} = u_{IVW_{c_i}}^{\nu_I} + K_i \sum_{j=1,\, j\neq i}^{m} E_{ij}\left(v_{IW_j}^{\nu_V} - v_{IW_j}^{\nu_V - 1}\right)$$

$$+ E_{ii}\left(v_{IW_i}^{\nu_V} - v_{IW_i}^{\nu_V - 1}\right) \tag{27}$$

Local-Simultaneous Coupling of LIL with a Finite Difference Boundary-Layer Method

The coupling of LIL with finite difference boundary-layer equations is described in great detail in Ref. 15. In the following equations the subscript c and the iteration index ν_V are neglected. In Eq. (27) the outblow velocities v_{IW} are substituted by Eq. (4) and discretized using central difference formulas for nonequidistant step sizes to obtain

$$u_{e_i} - \lambda_V D_{ii}(u_e\delta_1)_i = u_{IVW_i}^{\nu_I} + \sum_{j=1,\, j\neq i}^{m} D_{ij}\left[(u_e\delta_1)_j^{\nu_V - 1}\right.$$

$$\left. - (u_e\delta_1)_j^{\nu_V - 2}\right] - D_{ii}(u_e\delta_1)_i^{\nu_V - 1} \tag{28}$$

with

$$D_{ij} = a_{j+1}E_{i,j+1} + b_jE_{ij} + c_{j-1}E_{i,j-1} \tag{29}$$

and a, b, and c are given from Eqs. (14) and (15) and λ_V from Eq. (16). For simplification K_i is set to $K_i = 1$ and ρ_e is assumed to be constant for the outblow velocities in LIL. Because of the chosen discretization, the matrix $|D|$ is diagonally dominant as shown before in Fig. 1.

The unknown velocity u_e and displacement thickness δ_1 on the left-hand side of Eq. (28) are expressed by the stream-function formulation of the boundary-layer problem, $\psi(x, n) = \sqrt{\nu x u_0} f(x, n)$, using a coordinate transformation in the normal direction of $d\eta = (\sqrt{u_0/\nu x})\, dn$:

$$u_e = f_e' \tag{30}$$

$$\delta_1 = \int_0^\delta \left(1 - \frac{u}{u_e}\right) dn = \sqrt{\frac{\nu x}{u_0}}\left(\eta_e - \frac{f_e}{f_e'}\right) \tag{31}$$

where $'$ denotes the derivative with respect to n, and $u_0 = u_{e_{\mathrm{LIL}}}$, the reference velocity at the beginning of LIL coupling. Then LIL is obtained in the stream-function formulation:

$$EU_i f_{e_i} + (1 - EU_i\eta_{e_i}) f_{e_i}' = u_{IVW_i}^{\nu_I} + \sum_{j=1,\, j\neq i}^{m} D_{ij}\left[(u_e\delta_1)_j^{\nu_V - 1}\right.$$

$$\left. - (u_e\delta_1)_j^{\nu_V - 2}\right] - D_{ii}(u_e\delta_1)_i^{\nu_V - 1} \tag{32}$$

with

$$EU_i = \lambda_{V_i} D_{ii}\sqrt{\left(\frac{\nu x}{u_0}\right)_i} \tag{33}$$

For the boundary-layer solution, the finite difference method of Thiele[20] is used, which is based on Hermitian interpolation polynomials. The turbulent closure is approximated by the Cebeci-Smith model.[33] The boundary-layer equations are also written in the stream-function formulation and in transformed coordinates as mentioned earlier. For more detail see Ref. 20. Using backward discretization over x and Newton-Raphson linearization, the momentum equation for the boundary-layer flow is obtained:

$$(bf'')' + \left[0.5\hat{f} + (f_{i-1}\hat{f})\frac{x}{k_{i-1}}\right]f'' + \left[(2\hat{f}' - f_{i-1}')\frac{x}{k_{i-1}}\right]f'$$

$$+ \left[\hat{f}''\left(0.5 - \frac{x}{k_{i-1}}\right)\right]f + \left[\left(2\hat{f}_e' - f_{e_{i-1}}'\right)\frac{x}{k_{i-1}}\right]f_e'$$

$$= 0.5\hat{f}\hat{f}'' + \left(\hat{f}_e'^2 - \hat{f}'^2 - \hat{f}\hat{f}''\right)\frac{x}{k_{i-1}} \tag{34}$$

with $k_{i-1} = x_i - x_{i-1}$. Here, $i - 1$ refers to the solution from the upstream position and $\hat{}$ to the local solution from the previous Newton-Raphson iteration step. The continuity equation is identically fulfilled by using the stream-function formulation, and the

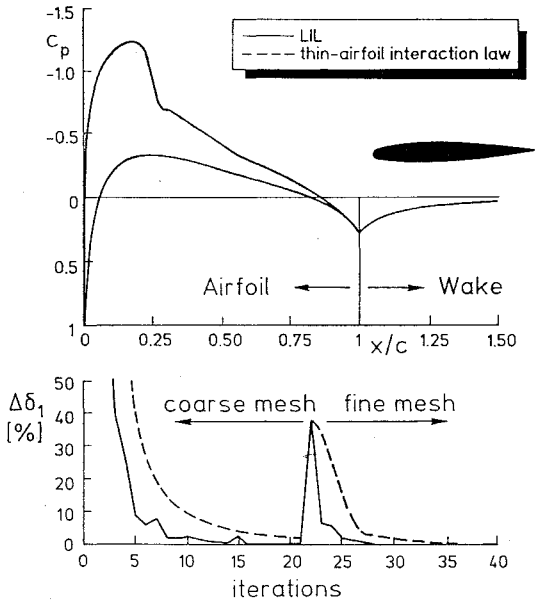

Fig. 9 Pressure coefficients and convergence behavior for transonic flow prediction over the NACA 0012 airfoil at $M_\infty = 0.7, Re_\infty = 9 \times 10^6$, and $\alpha = 2$ deg.

kinetic energy equation is replaced by the Crocco/van Driest formula given by Walz.[34]

The derivatives f''' and f'' are approximated by Hermitian polynomials of first order at all grid points in the normal direction. Thus, they linearly depend on f and f'. Using the inner boundary conditions at $\eta = 0$, on the surface

$$f = f' = 0 \tag{35}$$

on the wake stream/centerline

$$f = f'' = 0 \tag{36}$$

and LIL Eq. (32) for the outer boundary condition, a linear equation system for the unknowns f and f' follows from Eq. (34). The coefficient matrix is mainly of 2×2 block-tridiagonal structure and differs from the usual inverse matrix type only by the formulation of the right-hand side of the outer boundary condition. The matrix is solved by direct Gaussian elimination. Using the new local solution to replace $\hat{f}$, $\hat{f}'$, and $\hat{f}''$ in the Newton-Raphson linearization, we repeat the solution until local convergence is obtained. If this procedure has been performed for all streamwise positions, the boundary-layer sweep is finished.

Iteration Process and Test of Application

Starting from the compressible inviscid solution for u_{IVW} with $v_{IW} = 0$, several boundary-layer sweeps are performed. After each boundary-layer sweep, the outblow velocities used in LIL are updated, whereas the inviscid velocities remain unchanged. Experience with the quasisimultaneous coupling has shown that the boundary-layer sweeps do not have to be fully converged for each global iteration step with the inviscid code. Thus, only three sweeps are chosen to obtain the new outblow velocities that are prescribed as viscous boundary conditions for the next inviscid solution. The computation is complete when the required accuracies for the lift coefficient and the local displacement thicknesses are achieved.

To give an example of the convergence behavior of the quasisimultaneous coupling, the flow over the single-element airfoil NACA 0012 is predicted for Mach 0.7 and Reynolds number 9×10^6. In Fig. 9 the comparison of convergence behaviors is presented for LIL and the thin-airfoil interaction law application. The results of LIL show a clearly enhanced convergence due to the more appropriate influence coefficients. The calculations are for 22 iterations on a coarse mesh before switching to a fine mesh. Both results agree quite well with respect to the pressure distributions.

Conclusions

Results from the investigated test cases confirm the applicability of LIL for generating fast-converging IBL solutions for airfoil flows in low- and high-speed aerodynamics. The local-simultaneous coupling of an integral boundary-layer method with LIL was performed in the highly efficient code VILMA for low-speed multi-element airfoil flows. This code reduces computer time by more than 65% compared with the application of the conventional semi-inverse coupling technique, and due to the accurate influence coefficients of LIL, it converges faster than quasisimultaneous methods based on thin-airfoil interaction laws. The predicted results show good agreement with data from experiments below maximum lift, as well as realistic tendencies with accurate differences for changing flow parameters. For massive separated flows over strongly deployed flaps, or at maximum lift, the improvement of the physics of the method is still under investigation to obtain accurate results.

The first test for the quasi-simultaneous coupling of a finite difference boundary-layer method and a full potential method using LIL was presented for a transonic airfoil flow. The application of LIL shows an enhanced convergence behavior compared with the application of the thin-airfoil interaction law.

It appears that adequate coupling techniques are the fundamental principles for quickly converging IBL methods, which can then be used over a wide range of industrial applications. Shortcomings in the boundary-layer concept, however, sometimes necessitate the application of the more complete Navier-Stokes methods, especially for complex three-dimensional flows.

References

[1]Philips, E. H., "NASA/Langley Using Varied Approach to Develop Subsonic High Lift Devices," *Aviation Week & Space Technology*, Feb. 1992, p. 49.

[2]"High-Lift System Aerodynamics," Proceedings AGARD-CP-515, Sept. 1992.

[3]"Improvement of Aerodynamic Performance Through Boundary Layer Control and High Lift Systems," Proceedings AGARD-CP-365, Aug. 1984.

[4]"High Lift Aerodynamics," *Proceedings of the Royal Aeronautical Society* (Churchill College, Cambridge, England, UK), Royal Aeronatical Society (RAS), Dec. 1986.

[5]Le Balleur, J. C., "New Possibilities of Viscous-Inviscid Numerical Techniques for Solving Viscous Flow Equations with Massive Separation," *Proceedings of the 4th Symposium on Numerical and Physical Aspects of Aerodynamic Flows* (Long Beach, CA), CSULB, Jan. 1989.

[6]Carter, J. E., "A New Boundary-Layer Inviscid Iteration Technique for Separated Flow," AIAA Paper 79-1450, 1979.

[7]Le Balleur, J. C., "Strong Matching Method for Computing Transonic Viscous Flows Including Wakes and Separations. Lifting Airfoils," *La Recherche Aerospatiale*, No. 1981-3, 1981.

[8]Veldman, A. E. P., "New, Quasi-Simultaneous Method to Calculate Interacting Boundary Layers," *AIAA Journal*, Vol. 19, No. 1, 1981, pp. 79–85.

[9]Davis, R. T., and Werle, M. J., "Progress on Interacting Boundary-Layer Computations at High Reynolds Number," *Numerical and Physical Aspects of Aerodynamic Flows*, edited by T. Cebeci, Springer-Verlag, New York, 1982, pp. 187–210.

[10]Veldman, A. E. P., Lindhout, J. P. F., and de Boer, E., "VISIAN: A Viscous-Inviscid Strong-Interaction Analysis System," National Aerospace Lab., NLR TR 88081 L, The Netherlands, 1988.

[11]Edwards, D. E., and Carter, J. E., "A Quasi-Simultaneous Finite Difference Approach for Strongly Interacting Flow," *Numerical and Physical Aspects of Aerodynamic Flows III*, edited by T. Cebeci, Springer-Verlag, New York, 1985, pp. 126–142.

[12]Sorensen, J. N., "Prediction of Separated Flow Past Airfoil Using Viscous-Inviscid Interaction Technique," *La Recherche Aerospatiale*, No. 1988-3, 1988.

[13]Rothmayer, A. P., "Calculation of Laminar Separation Bubbles in the Wake Inflation/Deflation on Regime," *AIAA Journal*, Vol. 27, No. 9, 1989, pp. 1191–1199.

[14]Jakob, H., "Berechnung der ebenen Unterschallströmung um Mehrelementkonfigurationen zur Kopplung mit Grenzschichtverfahren einschließlich Nachlaufeinfluß," MBB GmbH, MBB Rep. TE2-1566, Bremen, Germany, 1987.

[15]Arnold, F., "Ein simultanes Lösungsverfahren mit exaktem Interaktionsgesetz zur Berechnung von inkompressiblen Profilströmungen," Ph.D. Thesis, Technische Universität Berlin, 1991; also *Fortschritt-Berichte VDI*, Reihe 7, Nr. 188, VDI-Verlag, Düsseldorf, Germany, 1991.

[16]Catherall, D., and Mangler, K. W., "The Integration of the Two-Dimensional Laminar Boundary-Layer Equations Past the Point of Vanishing Frictional," *Journal Fluid Mechanics*, Vol. 26, 1966, pp. 163–182.

[17]Henke, H., Müller, U. R., and Schulze, B., "A Viscous Inviscid Interaction Method for Use in Transonic Flutter Analysis," *International Forum on Aeroelasticity and Structural Dynamics* (Aachen, Germany), June 1993.

[18]Arnold, F., "VILMA-Berechnungsverfahren für viskose Strömungen um Spaltklappenprofile," Deutsche Airbus GmbH, DA Rep. EF-1904 Limited, Bremen, Germany, 1992.

[19]Dargel, G., "Ein Programmsystem für die Berechnung transsonischer Profil- und konischer Flügelströmungen auf der Basis gekoppelter Potential- und Grenzschichtlösungen," *Proceedings of the 8th DGLR Symposium STAB* (DLR, Köln-Porz), DGLR, DGLR Rep. 92-07, Bonn, Germany, 1992.

[20]Thiele, F., "Accurate Numerical Solutions of Boundary Layer Flows by the Finite Difference Method of Hermitian Type," *Journal of Computational Physics*, Vol. 27, 1978, pp. 138–159.

[21]Mertens, J., Klevenhusen, K. D., and Jakob, H., "Accurate Transonic Wave Drag Prediction Using Simple Physical Models," AIAA Paper 86-0512, 1986.

[22]Lighthill, M. J., "On Displacement Thickness," *Journal of Fluid Mechanics*, Vol. 4, 1958, pp. 383–392.

[23]Van-Dyke, M., "Higher-Order Boundary Layer Theory," *Annual Review of Fluid Mechanics*, Vol. 1, 1969, pp. 265–292.

[24]Whitfield, D. L., Swaffort, T. W., and Donegan, T. L., "An Inverse Integral Computational Method for Compressible Turbulent Boundary Layers," *Recent Contributions to Fluid Mechanics*, edited by W. Haase, Springer-Verlag, Berlin, 1982, pp. 294–302.

[25]Drela, M., "Two-Dimensional Transonic Aerodynamic Design and Analysis Using the Euler Equations," Massachusetts Inst. of Technology, GTL Rept. 187, Cambridge, MA, 1986.

[26]Van Ingen, J. L., "On the Calculation of Laminar Separation Bubbles in Two-Dimensional Incompressible Flow," AGARD-CP-168, 1975.

[27]Goradia, S. H., and Lyman, V., "Laminar Stall Prediction and Estimation of $c_{L(\max)}$," *Journal of Aircraft*, Vol. 11, 1974, pp. 528–536.

[28]Granville, P. S., "The Calculation of the Viscous Drag of Bodies of Revolution," Navy Dept., Rept. 849, 1953.

[29]McGhee, R. J., Beasley, W. D., and Somers, D. M., "Low-Speed Aerodynamic Characteristics of a 13-Percent-Thick Airfoil Section Designed for General Aviation Applications," NASA TM X-72697, 1977.

[30]Van den Berg, B., "Boundary Layer Measurements on a Two-Dimensional Wing with Flap," National Aerospace Lab., Data Rept., NLR TR 79009 U, The Netherlands, 1979.

[31]Thibert, J. J., "The GARTEUR High Lift Research Programme," AGARD-CP-515, 1993.

[32]Deutsche Aerospace Airbus, unpublished measurements in the Low Speed Wind Tunnel, Bremen, Germany, 1992.

[33]Cebeci, T., Clark, R. W., Chang, K. C., Halsey, N. D., and Lee, K., "Airfoils with Separation and the Resulting Wakes," *Proceedings of the 3rd Symposium on Numerical and Physical Aspects of Aerodynamic Flows* (Long Beach, CA), CSULB, Jan. 1985.

[34]Walz, A., *Boundary Layers of Flow and Temperature*, MIT Press, Cambridge, MA, 1969, Chap. 2.3, p. 65.